

Terahertz Spectroscopy and Modelling of Biotissue

by

Gretel Markris Png

Bachelor of Engineering (Electrical and Electronics Engineering, First Class Honours),
The University of Edinburgh, Scotland, UK, 1997

Master of Science (Electrical Engineering and Computer Science),
University of California at Irvine, USA, 2003

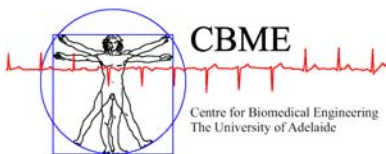
Thesis submitted for the degree of

Doctor of Philosophy

in

School of Electrical and Electronic Engineering,
Faculty of Engineering, Computer and Mathematical Sciences
The University of Adelaide, Australia

June, 2010



© 2010
Gretel Markris Png
All Rights Reserved



For Sheera

your love and belief in me have made this PhD journey possible

“Throughout the centuries, there were men who took first steps down new roads armed with nothing but their own vision.”

The Fountainhead by Ayn Rand (1905–1982)

Contents

<u>Heading</u>	<u>Page</u>
Contents	v
List of Figures	xvii
List of Tables	xxv
Abstract	xxvii
Statement of Originality	xxix
Publications	xxxi
Acknowledgements	xxxv
Conventions	xxxvii
Nomenclature	xxxix
Common acronyms used in this Thesis	xl
Common mathematical symbols and constants	xl
Chapter 1. Introduction and Motivation	1
1.1 Introduction	2
1.2 What is Terahertz?	2
1.3 The Historical Landscape of Terahertz Technology	2
1.3.1 The Forebears of Terahertz Technology	3
1.3.2 The Early Days of Terahertz Technology	7
1.4 Terahertz in Medicine and Biology	10
1.4.1 Terahertz Sensing of Proteins	12
1.4.2 Terahertz Sensing of Biotissue	12

1.5	Motivation for Thesis	17
1.5.1	Motivation 1: Interaction of Terahertz with Biotissue	18
1.5.2	Motivation 2: Sensing the Pathogens of Alzheimer’s Disease	19
1.6	Outline of Thesis	19
1.6.1	Summary of Contents in Appendices	22
1.7	Original Contributions	23
Chapter 2. An Overview of Terahertz Systems: Part 1		27
	Acronyms related to THz systems	28
2.1	Systems Not Based on EO/PC THz Generation	28
2.2	Continuous Wave THz Generation	29
2.2.1	Continuous Wave THz Detection	30
2.3	Tunable Gas Laser	31
2.4	Solid-State Semiconductor Systems	33
2.4.1	Solid-State Semiconductor THz Emitters	36
2.5	THz Sources Based on DFG	38
2.6	THz Sources Based on High-Frequency Oscillation	40
2.6.1	Gyrotron	40
	Gyrotron Applications	42
2.6.2	Backward-wave oscillator (BWO)	42
	BWO Applications	42
2.7	THz Sources Based on Electron Acceleration	44
2.7.1	Synchrotrons	44
	Synchrotron-Based Biological Applications	45
2.7.2	Free Electron Laser	47
2.8	Chapter Summary	49
Chapter 3. An Overview of Terahertz Systems: Part 2		51
	Acronyms and symbols related to THz systems	52
3.1	Overview of Pulsed THz-TDS Systems	54
3.1.1	Custom-Built Systems	54

3.1.2	Commercial Systems	56
3.2	Nonlinear Materials	58
3.2.1	Noncentrosymmetrical Crystals	59
3.3	Optical Harmonics: Second Harmonic Generation	60
3.3.1	Optical Rectification (OR)	61
3.4	The Pockels Effect (Linear Electro-Optic Effect)	62
3.4.1	Influence of the Pockels Effect on the Polarisation Axes	64
3.4.2	Absence of Applied External Field in EO Systems	67
3.5	Generation and Detection of Subpicosecond Pulses	67
3.5.1	Photodetectors for Picosecond Pulses: the Auston Switch	68
3.5.2	Subpicosecond EO Sampling System	69
3.6	Terahertz in Nonlinear Material: Čerenkov Sampling	71
3.7	Common Optical Components in Pulsed Systems	73
3.7.1	Ultrafast Laser	73
3.7.2	Amplitude Modulation: Mechanical Chopper	73
3.7.3	Delay Stage	74
3.7.4	Parabolic Mirrors	74
3.8	Photoconductive Antenna (PCA) THz System	75
3.8.1	Principle of Photoconductivity: THz Generation Using PCAs	77
3.8.2	Photoconductive THz Detection	82
3.8.3	New Dipole Antenna Materials and Designs	84
3.9	Electro-optic (EO) THz Generation	86
3.10	Electro-optic (EO) THz Detection	88
3.10.1	Aligning THz and Laser Pulses	89
3.10.2	Terahertz-Induced Polarisation Change	90
3.10.3	Circular Polarisation of a Signal	91
3.10.4	Wollaston Prism (WP)	91
3.10.5	Balanced Photodetectors and Lock-In Amplifier (LIA)	92
3.11	Variants of Pulsed THz-TDS Systems	93
3.12	Chapter Summary	94

Chapter 4. Review of Medical Spectroscopy and Imaging	95
4.1 Medical Diagnostic Technologies	96
4.2 What Causes Spectral Fingerprints?	97
4.3 Infrared Medical Spectroscopy	98
4.3.1 Common Modalities and Analytical Tools for IR Spectroscopy . .	104
4.3.2 Applications of Infrared Spectroscopy	105
Infrared Spectroscopy of Cells	105
Infrared Spectroscopy of Skin	107
Infrared Spectroscopy of Deep Biotissue	109
Infrared Spectroscopy and Imaging of Infant Brains	110
Infrared Spectroscopy of Blood and Blood Vessels	111
4.4 Microwave Medical Spectroscopy	112
4.4.1 Common Modalities of Microwave Spectroscopy	113
4.4.2 Applications of Microwave Spectroscopy	114
4.5 Terahertz Medical Spectroscopy	116
4.5.1 Water Absorption in the THz Frequency Range	116
The Effect of Water Vapour in the THz Frequency Range . .	118
The Effect of Liquid Water in the THz Frequency Range . . .	120
4.5.2 Terahertz Studies of Biomolecules	122
Biomolecules in Solution	125
Terahertz Spectroscopy of Blood	127
Techniques for Improving SNR of THz Liquid Spectroscopy	127
4.5.3 Pharmaceutical Quality Control using THz	128
4.5.4 Terahertz Biotissue Studies	129
Problems Involving Excised Biotissue	129
4.6 Chapter Summary	131
Chapter 5. Impact of Fresh Biotissue Hydration on Terahertz Spectroscopy	133
5.1 Introduction	134
5.1.1 Motivation	134
5.1.2 Objective Summary	135

5.1.3	Location of Experimental Work	136
5.2	Terahertz Data Acquisition and Analysis	136
5.2.1	Terahertz Equipment	136
	Nitrogen Purging	136
	Types of Measured Signals	137
5.2.2	System Bandwidth and Dynamic Range	139
5.2.3	Terahertz Data Analysis	140
	Dependence of Optical Properties on Thickness	143
5.3	Sample Preparation Techniques	143
5.3.1	Fresh Biotissue Excision, Slicing and Storage	143
	Slicing Tools	144
5.3.2	Sample Transportation and Priming Prior to Measurements	146
5.3.3	Mounting Fresh Biotissue for Measurement	146
	Mounting Plates	147
5.4	Results and Discussion	147
5.4.1	Changes Over Time	148
	Dehydration of Biotissue in Nitrogen-Purged Atmosphere	150
5.4.2	Errors in Optical Properties Due to Thickness Variations	152
5.5	Lyophilisation: A Solution to Biotissue Variability	153
5.5.1	Common Preservation Methods for Biotissue	154
5.5.2	Why Lyophilisation?	155
5.5.3	Lyophilising and Mounting Biotissue for Measurement	156
5.5.4	Problems Encountered with Lyophilisation	157
5.5.5	Comparison: Lyophilised and Fresh Biotissue	158
5.5.6	Necrotic Samples as a Gauge for Biotissue Freshness	160
5.5.7	Comparison: Necrotic, Lyophilised and Fresh Biotissue	161
5.6	Conclusion	162
5.6.1	Future Work	162
5.7	Chapter Summary	166

Chapter 6. Terahertz-Based Analysis of Protein Plaques in Biotissue **167**

6.1	Introduction	168
6.1.1	Motivation	168
6.1.2	Objective Summary	169
6.1.3	Location of Experimental Work	169
6.2	Background of Alzheimer’s Disease	170
6.2.1	Folding of β -Pleated Sheets	172
6.2.2	Diagnosis of Alzheimer’s Disease (AD)	172
6.2.3	Atrophy in Brains Afflicted with Alzheimer’s Disease	175
6.3	Background into Brain Samples Used	175
6.3.1	Pathological Analysis of Biotissue	177
6.4	Sample Preparation	179
6.4.1	Identifying Brain Regions	179
6.4.2	Extraction of Biotissue	183
6.4.3	Slicing Tools	185
6.4.4	Mounting Snap-Frozen Biotissue for Measurement	185
6.4.5	Terahertz Data Analysis	189
6.5	Results and Discussion	189
6.5.1	Challenges	193
	Handling Issues	193
	Physical Condition of Brains	193
	Measurement Temperature	193
	Small Sample Set	195
6.6	Conclusion	195
6.6.1	Future Work	195
6.7	Chapter Summary	196

Chapter 7. Terahertz Spectroscopic Differentiation of Biological Microstructure 197

7.1	Introduction	198
7.1.1	Motivation	198
7.1.2	Objective Summary	199
7.1.3	Location of Experimental Work	199

7.2	Background to Biological Sub-Systems	200
7.3	Gels Containing β -Pleated Sheets	200
7.3.1	What is β -Lactoglobulin?	201
	Thermal Gelation	201
7.3.2	Influence of pH on Microstructure Formation in Gels	201
7.4	Synthesising β -Lactoglobulin Gels	206
7.4.1	Synthesising β -Lactoglobulin Solutions	207
7.4.2	Verifying Microstructures in Gels used in this Study	208
7.5	Terahertz Spectroscopic Measurements and Results	208
7.5.1	Rayleigh Scattering	211
7.6	Results	213
7.6.1	Differentiation of Structures	213
7.6.2	Influence of Sample Preparation and Measurement Conditions	217
	Influence of Freezing Rate	217
	Influence of Sample Holder	218
	Influence of Temperature	218
7.7	Conclusion	221
7.7.1	Future Work	221
7.8	Chapter Summary	221
Chapter 8. Scattering from Subwavelength Fibrils in the Terahertz Regime		223
8.1	Introduction	224
8.1.1	Motivation	224
8.1.2	Objective Summary	225
8.1.3	Location of Experimental Work	226
8.2	Brief Review of Scattering-Related Literature	226
8.3	Overview: Mie Scattering	228
8.3.1	Definition: An Infinitely Long Right Circular Cylinder	228
8.3.2	Analytical (Exact) Solutions for Mie Scattering	229
8.4	Fibrillar Samples and Experiment	230
8.5	Experimental Results	232

8.5.1	Observations From the Perpendicular Samples	233
8.5.2	Observations From the Parallel Samples	233
8.6	Comparison of Experimental and Analytical Results	235
8.6.1	Optical Properties of Bulk Glass	236
8.6.2	Optical Properties of Bulk Fibreglass Cloth	236
8.6.3	Comparison of Bulk Optical Properties	236
8.6.4	Scattering Cross Section	237
8.6.5	Modelling an Array with Analytical Solutions	238
8.6.6	Limitations of the Analytical Solutions	240
8.7	Full-Wave Electromagnetic Field Solver	241
8.7.1	The HFSS Model	241
8.7.2	Calculation of S-Parameters	244
8.8	Comparison of Experimental and Numerical Results	245
8.8.1	Shape of Plots at Lower THz Frequencies	245
8.8.2	Shape of Plots at Higher THz Frequencies	246
8.8.3	Influence of Overlapping Cylinders in the Array	248
8.9	Verifying Consistency in Periodic Models	248
8.9.1	Field Overlay Patterns	251
	Non-Periodic HFSS Model	251
	Comparison of Field Overlay Patterns	251
8.10	Precautions Needed When Using HFSS	254
8.11	Conclusion	255
8.11.1	Future Work	256
8.12	Chapter Summary	256
Chapter 9. Modelling Terahertz Propagation in Stratified Media		259
9.1	Introduction	260
9.1.1	Motivation	260
9.1.2	Objective Summary	261
9.2	Review of Modelling Methods	261
9.3	Transmission Line Model for THz Propagation	262

9.4	Optical (Dielectric) Properties of Biotissue	266
9.4.1	Infrared and Submillimeter Regions	266
9.4.2	Microwave Region	267
9.4.3	Interpolating Optical Properties: Between Microwave and THz	269
9.5	Test and Results	272
9.5.1	Test Conditions: Empirical and Simulated	272
9.5.2	Simulation Results using the Transmission Line Model	274
9.6	Feasibility of <i>In Vivo</i> Terahertz Diagnosis of the Head	277
9.7	Conclusion	279
9.7.1	Future Work	280
9.8	Chapter Summary	280
 Chapter 10. Conclusion and Recommendations		281
10.1	Introduction	282
10.2	Thesis Conclusions	282
10.2.1	Review of Terahertz Systems	282
10.2.2	Review of Medical Spectroscopy	283
10.2.3	Experiments: Analysis of Biotissue Hydration	283
10.2.4	Experiments: Differentiating Health of Biotissue	284
10.2.5	Experiments: Differentiating Microstructures in Gels	285
10.2.6	Experiments and Modelling: Scattering from Cylinders	286
10.2.7	Modelling: Propagation and Scattering from Layers	287
10.3	Recommendations for Future Work	288
10.3.1	Biotissue Hydration	289
10.3.2	Differentiating Health of Biotissue	289
10.3.3	Differentiating Microstructures in Gels	290
10.3.4	Scattering from Cylinders	290
10.3.5	Propagation and Scattering from Layers	291
10.3.6	Preliminary Study 1: Pseudo-Phase Contrast	291
10.3.7	Preliminary Study 2: Polymer Hole Arrays	291
10.3.8	Preliminary Study 3: Etalon Removal	292
10.3.9	Preliminary Study 4: Inverse Problems	292
10.4	Summary of Original Contributions	292
10.5	Chapter Summary	294

Appendix A. Preliminary Studies	295
A.1 Preliminary Study 1: Pseudo-Phase Contrast	296
A.1.1 Preliminary Results	296
A.1.2 Future Work	300
A.2 Preliminary Study 2: Polymer Hole Arrays	300
A.2.1 Preliminary Evaluation	301
A.2.2 Future Work	303
A.3 Preliminary Study 3: Etalon Removal	304
A.3.1 Proposed Algorithm	305
A.3.2 Preliminary Results	306
A.3.3 Future Work	309
A.4 Preliminary Study 4: Inverse Problems	309
A.5 Appendix Summary	310
Appendix B. Nonlinearity in Materials	311
B.1 Susceptibility χ	312
B.1.1 Sample Values of $\chi^{(2)}$	312
B.2 Noncentrosymmetrical Crystals	313
B.3 Introduction to Nonlinear Crystal Geometry	315
B.3.1 Miller Index	315
B.3.2 Bravais Lattice	316
B.3.3 Point Groups	317
B.3.4 Dependence of THz Generation on Crystal Properties	318
Appendix C. Main and Auxiliary Equipment for Terahertz Measurements	319
C.1 Components of THz-TDS Systems Used	320
C.2 Hank's Buffer	320
Appendix D. Mathematical Derivation of the Complex Refractive Index	325
D.1 Derivation of the Complex Refractive Index $\hat{n}(\omega)$	326
D.1.1 Complex Refractive Index $\hat{n}(\omega)$	326
D.1.2 Explanation of Variables Used in Equation (5.16)	327

D.2	Derivation of the Real Refractive Index $n(\omega)$	328
D.2.1	The Fresnel Equations	328
D.2.2	Real Refractive Index $n(\omega)$	329
Appendix E. Neuropsychological Assessment of Alzheimer’s Disease		331
E.1	The Modified Mini Mental State (3MS) Examination	332
E.2	Types of Dementia	332
Appendix F. The Mathematics of Scattering-Related Theories		335
F.1	Introduction	336
F.2	Spherical Scatterers	336
F.2.1	Plane Wave Equation in Cartesian Coordinates	336
F.2.2	Plane Wave Equation of a Sphere	337
F.2.3	Solution of $\Phi(\phi)$	337
F.2.4	Solution of $\Theta(\theta)$	337
F.2.5	Solution of $R(r)$	337
F.2.6	Solution of $\psi(r, \theta, \phi)$	338
F.2.7	Vector Spherical Harmonics	338
F.2.8	Equation of a Plane Wave in Vector Spherical Harmonics	339
F.3	Cylindrical Scatterers	340
F.3.1	Plane Wave Equation of a Cylinder	340
F.3.2	Vector Cylindrical Harmonics	341
F.3.3	Case I: Incident E Parallel to xz Plane, H Perpendicular to xz Plane	342
	Internal Field in Vector Cylindrical Harmonics for Case I . . .	343
	Scattered Field in Vector Cylindrical Harmonics for Case I . . .	344
	Large distances from cylinder for Case I (asymptotic scattered field)	345
F.3.4	Case II: Incident E Perpendicular to xz Plane, H Parallel to xz Plane	345
	Case II: Scattered Field in Vector Cylindrical Harmonics . . .	346
	Large distances from cylinder for Case II (asymptotic scattered field)	347

Contents

F.4	Scattering Matrix of a Cylinder	347
F.4.1	Relationship Between Amplitudes of Incident and Scattered Fields for a Cylinder	348
	Scattered Field in Forward or Backward Scattering Plane . .	348
	Incident Wave Normal to z Axis ($\theta = 90^\circ$)	348
F.5	Efficiencies for a Cylinder	349
F.5.1	Efficiencies of a Cylinder for Case I: Parallel Incident Electric Field	349
F.5.2	Efficiencies of a Cylinder for Case II: Perpendicular Incident Elec- tric Field	350
F.5.3	Small Particle Limit	350
F.6	Rayleigh-Gans Scattering	350
F.7	Geometric Optics	351
F.8	Beckmann Distribution Function	352
F.8.1	Application of the Beckmann Distribution Function	353
Appendix G. General Solution of the Helmholtz Equation		357
G.1	General Solution of the Helmholtz Equation	358
Appendix H. Data Processing Algorithms		363
H.1	Data Processing Common to All Measured Datasets	364
H.1.1	List of Source Code Files	365
H.2	Algorithms for Modelling Scattering	366
H.2.1	Source Code	366
H.3	Data Processing for Modelling Stratified Layers	373
H.4	Algorithms for Optical (Dielectric) Properties	381
H.4.1	Source Code	381
H.5	Algorithms for Plotting HFSS Field Overlay Patterns	385
H.6	Algorithm for Pseudo-Phase Contrast	385
Bibliography		391
Index		445
Résumé		453

List of Figures

<u>Figure</u>		<u>Page</u>
1.1	Electromagnetic spectrum	3
1.2	The Herschel spacecraft	6
1.3	The ALMA interferometer antenna arrays	7
1.4	Study of leaf hydration using THz	14
1.5	Chocolate causes cavity?	15
1.6	Identification of tumours in formalin-fixed liver	15
1.7	Identification of skin cancer	16
1.8	Portable THz technology	17
1.9	Thesis structural flow chart	20
<hr/>		
2.1	A commercial THz imaging system	30
2.2	A THz pyroelectric camera	31
2.3	Continuous wave THz images	32
2.4	Continuous wave THz system based on a gas laser	34
2.5	Continuous wave THz system based on a Gunn diode	35
2.6	Quantum cascade laser (QCL)	37
2.7	Continuous wave THz spectroscopic system based on a QCL	38
2.8	Continuous wave THz imaging system based on a QCL	38
2.9	Gyrotrons	41
2.10	JET and ITER tokamaks	43
2.11	Backward-wave oscillator	43
2.12	Examples of synchrotrons	45
2.13	The Australian Synchrotron	46
2.14	High resolution images from a synchrotron	47
2.15	Examples of free electron lasers	48

List of Figures

2.16	Continuous wave THz system based on a FEL	49
<hr/>		
3.1	Types of pulsed THz systems	55
3.2	Examples of commercial pulsed THz systems	56
3.3	Examples of portable commercial pulsed THz systems	57
3.4	Example of a fibre-coupled commercial pulsed THz system	57
3.5	The Pockels Effect in a noncentrosymmetrical crystal	65
3.6	The Auston switch	68
3.7	Electro-optic sampling system for detecting electrical transients	70
3.8	A typical chopper and delay stage in a THz system	74
3.9	Four parabolics used to focus THz radiation to a point	75
3.10	Development of the photoconducting dipole antenna	76
3.11	First long-range PCA system	78
3.12	Photoconductivity in PCAs	79
3.13	Improvements to PCA designs	85
3.14	Novel PCA construction	86
3.15	Examples of crystals used in EO THz generation	88
3.16	Alignment of THz and laser pulses for EO THz detection	90
3.17	Wollaston prism (WP)	92
3.18	Photodetectors	93
<hr/>		
4.1	A comparison of the IR spectra of styrene and polystyrene	101
4.2	Infrared, Raman, and NMR spectra of styrene	102
4.3	Infrared spectroscopy of cervical cancer cells	107
4.4	Infrared spectroscopy of synthetic skin	108
4.5	Phantoms for IR spectroscopy	109
4.6	Infrared spectroscopy of biotissue	110
4.7	Infrared spectroscopy of human infant brains	111
4.8	Infrared spectroscopy of blood vessels	112

4.9	Example of a microwave spectrometer	114
4.10	Microwave imaging of a breast phantom	117
4.11	Water vapour lines in the THz frequency range	120
4.12	Terahertz absorption by liquid water	121
4.13	Comparison of α of opaque and transparent materials in the THz frequency range	121
4.14	Structural differences in biomolecules	124
4.15	Examples of liquid cells	126
4.16	Differentiating biotissue in the THz frequency range	131
<hr/>		
5.1	Nitrogen-purged test chamber	137
5.2	Time and frequency domain representations of THz data	138
5.3	System layout for noise measurement	139
5.4	Storage of fresh biotissue after excision	144
5.5	Examples of commercial biotissue slicing apparatus	145
5.6	Custom-built biotissue slicer	145
5.7	Double plate sample holder	148
5.8	Single plate sample holder	148
5.9	Noise floor	149
5.10	Irrelevant α	149
5.11	Improvement to bandwidth and system dynamic range	150
5.12	Dehydration rates in biotissue	151
5.13	Visual observation of biotissue dehydration over time	152
5.14	Uncertainties due to changes in thickness	153
5.15	Phase diagram of water	155
5.16	Lyophiliser	156
5.17	Visual and physical changes in lyophilised biotissue	157
5.18	Rejected lyophilised samples	158
5.19	Nitrogen-dried fresh diaphragm	158
5.20	Absorption coefficient α of fresh versus lyophilised biotissue	159

List of Figures

5.21	Optical images of rat colon samples	163
5.22	Terahertz absorption coefficients α of nitrogen-dried fresh, lyophilised, and nitrogen-dried necrotic samples	164
5.22	Terahertz absorption coefficients α of nitrogen-dried fresh, lyophilised, and nitrogen-dried necrotic samples (continued)	165
<hr/>		
6.1	Prevalence of AD as the cause of dementia	170
6.2	Plaques and tangles	171
6.3	Protein folding process	173
6.4	Uptake of PIB in healthy and AD-afflicted brains	174
6.5	Atrophy in an AD-afflicted brain	176
6.6	Extract from the database of donations	177
6.7	Coronal brain slices	178
6.8	Annotated views of the left and right brain hemispheres	182
6.9	Snap-frozen brain slice	183
6.10	Extraction of cores from a snap-frozen brain slice	184
6.11	Two views of brain disks	186
6.12	Picometrix T-ray 2000 System with a nitrogen-purged chamber	186
6.13	THz system setup for measuring brain disks	187
6.14	Effect of vacuum evacuation on brain samples	188
6.15	THz absorption coefficients $\alpha(\omega)$ of various healthy and diseased brain disks 2.41 ± 0.05 mm thick	191
6.16	THz absorption coefficients $\alpha(\omega)$ of various healthy and diseased brain disks 3.1 ± 0.6 mm thick	192
6.17	Poor quality core from a healthy donor	194
6.18	Photograph and scanning electron micrograph (SEM) of blood vessels in the neocortex of two male donors	194
<hr/>		
7.1	Formation of fibrillar and globular microstructures in β -lg gels	202
7.2	Schematic representations of microstructures in β -lg gels	204

7.3	Atomic force micrographs and electron micrograph of microstructures in β -lg gels	204
7.3	Atomic force micrographs and electron micrograph of microstructures in β -lg gels (continued)	205
7.4	Optical image of frozen gel	207
7.5	Electron micrographs of gels synthesised in this study	209
7.6	Picometrix T-ray-2000 system used in this study	209
7.7	Custom PCA system used in this study	210
7.8	Extinction coefficients of β -lg gels and solutions	214
7.9	Refractive indices of β -lg gels and solutions	215
7.10	Normalised Rayleigh scattering efficiencies $Q_{\text{sca}}(\omega)$ versus extinction coefficients $\alpha(\omega)$ of fibrils and globules	216
7.11	Comparison of slow and snap-frozen pH 4 gels	219
7.12	Effect of lyophilisation on extinction coefficient	220
7.13	Influence of measurement temperature on extinction coefficients	220

8.1	Schematic diagram of cylinders' orientations with respect to the THz polarisation	229
8.2	Experimental setup	232
8.3	Experimental results	234
8.4	Plots over a wider range of frequencies	235
8.5	Calculated $C_{\text{sca},\parallel}$ and $C_{\text{sca},\perp}$	238
8.6	Far-field radiation patterns	239
8.7	Influence of array factor on C_{sca}	240
8.8	Near-periodic HFSS model and its radiation boundaries	242
8.9	Near-periodic cylindrical array in airbox	243
8.10	S-parameters of a 2 port network	245
8.11	S_{21} plots for both orientations with 1 μm space between adjacent cylinders	246
8.12	S_{21} plots for both orientations with 1, 5 and 10 μm spaces between adjacent cylinders	247
8.13	S_{21} plots for single-layered and double-layered arrays	249

List of Figures

8.14	Comparison of similar periodic models	250
8.15	Field overlay and directivity patterns	252
8.16	Non-periodic parallel HFSS model	253
8.17	Non-periodic perpendicular HFSS model	254
<hr/>		
9.1	Schematics of stratified medium and tissue layers in the head	263
9.2	Optical properties of adipose tissue and skin	270
9.3	Interpolating optical properties of skin	270
9.4	Reflected signals from the skin of the forearm	273
9.5	Transmission line model simulated reflected signal from 7 tissue layers in the head	275
9.6	Third to sixth reflections from the transmission line model	276
9.7	Seventh and eighth reflections from the transmission line model	278
<hr/>		
A.1	Extracting the time response from various pixels in the 3D dataset	297
A.2	Alternative representations of THz data	298
A.3	Examples of metal hole arrays	301
A.4	Modelling periodic hole arrays in HFSS	302
A.5	Effect of modifying cell and hole dimensions	303
A.6	PDMS hole array	304
A.7	Performance comparison of algorithms for a multilayered test scenario	307
A.8	Performance comparison of algorithms for a single layered test scenario	308
<hr/>		
B.1	Relationship between applied electric field strength and emitted polari- sation density	312
B.2	Miller indices for planes	316
B.3	Miller indices for directions	316
B.4	Schematic of the 14 Bravais lattices	317

F.1	Optical properties of rat ventral skin, with and without shaving	353
F.2	Magnitudes of the reflected THz signal at 1.225 THz	355
F.3	Comparison between the incident THz signal and the simulated reflected signal using the Beckmann distribution function	356
H.1	Flow chart of common data processing techniques used in this Thesis . .	364

List of Tables

<u>Table</u>	<u>Page</u>
4.1	An extract of the IR correlation table of functional groups 100
4.2	Discovery of water vapour lines 119
6.1	Examples of human brain diseases caused by protein misfolding and aggregation 171
6.2	Microscopic Brain Report 180
6.3	List of cases used in this study 181
9.1	Summary of variables used in the 4-term Cole-Cole model 271
9.2	Optical properties compiled or interpolated from literature for the 0.1–1 THz frequency range 271
9.3	Propagation and cumulative travel times 277
B.1	Examples of $\chi^{(2)}$ of several THz-related crystals 314
B.2	Examples of nonlinear THz-related crystals 314
B.3	Bravais lattices 317
B.4	Point groups using the Hermann-Mauguin convention 318
C.1	List of equipment used at the University of Adelaide for experiments reported in this Thesis 321
C.2	List of equipment used at the University of Adelaide for experiments reported in this Thesis 321
C.3	List of equipment used at Rensselaer Polytechnic Institute (RPI) for experiments reported in this Thesis 322
C.4	List of equipment used at the University of Leeds for experiments reported in this Thesis 323
E.1	Modified Mini-Mental State (3MS) Examination 333
E.1	Modified Mini-Mental State (3MS) Examination (continued) 334

List of Tables

H.1	MATLAB source code files for performing common data processing . . .	365
H.2	MATLAB source code files for modelling scattering	366
H.3	MATLAB source code files for interpolating and extrapolating	381
H.4	MATLAB source code files for writing to and reading from HFSS	386

Abstract

Pulsed terahertz (THz, or T-ray) research has burgeoned since its inception in the mid 1980s when the first pulses of THz radiation were emitted via electro-optic sampling. At the time, this discovery was a milestone for time domain spectroscopy because existing microwave and Fourier Transform Infrared (FTIR) spectrometers were not sensitive in the 0.1–10 THz frequency range. However, it would take several years before THz generation would become practical for spectroscopic use. In recent years, THz research has progressed to such a great extent that THz generation and detection techniques are now reliable and relatively low-cost, therefore THz has the potential to be used in a vast array of real-world applications ranging from security reinforcement (detection of weapons and explosives) to medical diagnosis (identifying melanomas). Indeed many bodies of research work have successfully demonstrated the efficacy of THz, although many challenges still exist before THz matures beyond the realm of research into everyday life.

This Thesis focuses on the area of THz spectroscopy and modelling of biotissue, with the aim of broadening the application of THz in medicine, particularly in the early diagnosis of Alzheimer's disease (AD). Since the nature of biotissue is complex, THz measurements of biotissue are prone to variability. Therefore, this Thesis includes the study of simpler biological analogues that mimic aspects of biotissue.

The work described in this Thesis makes five major novel contributions to THz research of biotissue: *(i)* the exploration of hydration and storage issues in freshly excised biotissue prior and during THz measurements; *(ii)* the use of snap-frozen biotissue in THz measurements for the purpose of investigating the plausibility of utilising THz sensing to distinguish between healthy and AD-afflicted human brain tissue; *(iii)* the use of THz spectroscopy to non-destructively differentiate between soft protein microstructures containing features of one of the known fibrillar pathogens of AD; *(iv)* the use of THz spectroscopy and full-wave electromagnetics simulation to study scattering from fibrillar structures akin to fibrillar pathogens of AD; and *(v)* transmission line modelling of THz propagation and reflection from stratified tissue layers in the human head.

The first part of this Thesis provides a historical review of the development of THz technology, with emphasis on the contributions of infrared (IR) and microwave research towards the realisation of the various THz generation and detection techniques available today. The various techniques are briefly reviewed prior to a thorough discussion of the types of THz generation and detection techniques used in this Thesis: electro-optic and photoconductive. A review of relevant IR, microwave, and THz medical research completes the first part of this Thesis.

In the second part of this Thesis, novel THz measurements of biotissue are presented and their results discussed. Experiment protocols for the handling and storage of excised biotissue are highlighted to emphasise how storage and hydration can severely alter THz measurements. Novel alternative sample preparation techniques, in the form of lyophilisation and snap-freezing, are presented. Terahertz spectroscopic comparison of healthy and AD-afflicted human tissue reveals promise for a future THz diagnostic tool, but highlights the need to investigate simplified biotissue analogues, such as skin, fat, and proteins. This need leads to the third part of this Thesis.

The third part of this Thesis involves THz spectroscopic study of one analogue of AD-afflicted biotissue: synthetically manufactured microstructures that resemble the proteins associated with AD. Terahertz differentiation of this microstructure from one with a dissimilar shape is revealed, suggesting a new non-destructive application for THz spectroscopy in biomedicine. The mechanism behind the differentiation is believed to be that of scattering, thus the next part of this Thesis explores scattering from more controlled test samples.

The penultimate part of this Thesis utilises a full-wave electromagnetics simulator to explain THz scattering from custom-built fibrillar structures. The novel use of the simulator allows a more accurate means of studying THz scattering, resulting in better agreement between measurement and simulation. The extra dimension of information that mathematical simulation provides leads to the final part of this Thesis, where a feasibility study is performed on the use of THz spectroscopy to study tissue layers in the head, with the aim of determining whether current THz systems can be used for *in vivo* diagnostic studies of tissue layers underneath the skin.

The contributions of this Thesis are important steps in advancing the use of THz in medicine, paving the way for the next generation of experimental and mathematical modelling studies of THz interaction with biotissue, in order to develop reliable THz diagnostic tools of the future.

Statement of Originality

This work contains no material that has been accepted for the award of any other degree or diploma in any university or other tertiary institution to Gretel Markris Png and, to the best of my knowledge and belief, contains no material previously published or written by another person, except where due reference has been made in the text.

I give consent to this copy of my Thesis, when deposited in the University Library, being made available for loan and photocopying, subject to the provisions of the Copyright Act 1968.

I also give permission for the digital version of my Thesis to be made available on the web, via the University's digital research repository, the Library catalogue, the Australasian Digital Theses Program (ADTP) and also through web search engines, unless permission has been granted by the University to restrict access for a period of time.

Signed

8 June 2010

Date

Publications

Journals

- PNG-G, FALCONER-R, FISCHER-B, ZAKARIA-H, MICKAN-S, MIDDELBERG-A AND ABBOTT-D (2009a). Terahertz spectroscopic differentiation of microstructures in protein gels, *Optics Express*, **17**(15), pp. 13102–13115. [1.7](#), [8.6.5](#), [3](#)
- PNG-G, FLOOK-R, NG-B. W.-H AND ABBOTT-D (2009c). Terahertz spectroscopy of snap-frozen human brain tissue: an initial study, *Electronics Letters*, **45**(7), pp. 343–345. [1.7](#), [2](#)
- PNG-G, CHOI-J.-W, NG-B. W.-H, MICKAN-S, ABBOTT-D AND ZHANG-X.-C (2008a). The impact of hydration changes in fresh bio-tissue on THz spectroscopic measurements, *Physics in Medicine and Biology*, **53**(13), pp. 3501–3517. [1.7](#), [7.5](#), [1](#)
- WITHAYACHUMNANKUL-W, PNG-G, YIN-X.-X, ATAKARAMIANS-S, JONES-I, LIN-H, UNG-B, BALAKRISHNAN-J, NG-B. W.-H, FERGUSON-B, MICKAN-S, FISCHER-B AND ABBOTT-D (2007). T-ray sensing and imaging, *Proceedings IEEE*, **95**(8), pp. 1528–1558. [1.7](#), [5](#)

Journal Paper Under Peer-Review

- PNG-G, STRINGER-M, FUMEAUX-C, MILES-R, AND ABBOTT-D (2010). Terahertz spectroscopy and numerical analysis of scattering from subwavelength fiberglass arrays. Submitted to *Optics Express* for peer-review.

Refereed Conferences

- PNG-G, FLOOK-R, NG-B. W.-H AND ABBOTT-D (2009b). Terahertz spectroscopy of misfolded proteins in bio-tissue, *Proc. 34th International Conference on Infrared, Millimeter, and Terahertz Waves (IRMMW-THz)*, 21–25 September 2009, Busan, South Korea, article number 0506. **(Invited Talk)** [1.7](#), [2](#)

- PNG-G, STRINGER-M, NG-B. W.-H, ABBOTT-D AND MILES-R (2008b). Orientation dependence of THz scattering from cylindrical strands, *Proc. 33rd International Conference on Infrared, Millimeter, and Terahertz Waves (IRMMW-THz)*, Pasadena, CA, USA, article number 1380. [1.7, 4](#)
- PNG-G, NG-B. W.-H, CHOI-J.-W, ZHANG-X.-C AND ABBOTT-D (2007). Influence of surface clutter on THz spectroscopy of skin, *Proc. Joint 32nd International Conference on Infrared and Millimetre Waves, and 15th International Conference on Terahertz Electronics (IRMMW-THz)*, **1**, Eds: M. Griffin, P. Hargrave, T. Parker and K. Wood, 3–7 September 2007, Cardiff, UK, pp. 565–566. [F.1](#)
- PNG-G, NG-B. W.-H, MICKAN-S, ABBOTT-D, CHOI-J.-W, SENGUPTA-S, AND WILKE-I (2006). Creams and oils: Possible THz coupling media for rough surfaces?, *Proc. Joint 31st International Conference on Infrared and Millimetre Waves, and 14th International Conference on Terahertz Electronics (IRMMW-THz)*, 18–22 September 2006, Shanghai, China, pp. 445.
- PNG-G, CHOI-J.-W, GUEST-I, NG-B. W.-H, MICKAN-S, ABBOTT-D AND ZHANG-X.-C (2006). Molecular and structural preservation of dehydrated bio-tissue for THz spectroscopy, *Proc. SPIE Smart Materials, Nano- and MicroSmart Systems*, **6416**, Ed: D. Abbott, 11–13 December 2006, Adelaide, Australia, article number 64160W.
- PNG-G, MICKAN-S AND ABBOTT-D (2005a). The potential use of T-rays in diagnosing the head and brain, *Proc. International Workshop on Terahertz Technology*, Ed: M. Tonouchi, 16–18 November 2005, Osaka, Japan, pp. 99–100. [1.7, 5](#)
- PNG-G, MICKAN-S AND ABBOTT-D (2005b). Simulation of terahertz radiation in stratified media, *Proc. SPIE Photonics: Design Technology, and Packaging II*, **6038**, Ed: D. Abbott, 11–14 December 2005, Brisbane, Australia, article number 60380M. [1.7, 5](#)
- RAINSFORD-T, PNG-G, WITHAYACHUMNANKUL-W, FERGUSON-B, MICKAN-S AND ABBOTT-D (2005). T-rays in biomedicine and security, *Proc. 18th Annual Meeting of the IEEE Lasers and Electro-Optics Society (LEOS)*, Eds: D. Novak, P. Juodawlkis, A. Nirmalathas, 22–28 October 2005, Sydney, Australia, pp. 116–117. **(Invited Talk)**
- PNG-G, MICKAN-S, RAINSFORD-T AND ABBOTT-D (2004). Terahertz phase contrast imaging, *Proc. SPIE Smart Structures, Devices, and Systems II*, **5649**, Ed: S. Al-Sarawi, February 2004, Sydney, Australia, pp. 768–777. [1.7, 6](#)

Non-Refereed Conferences

PNG-G, FLOOK-R, NG-B. W.-H AND ABBOTT-D (2009). Terahertz spectroscopy of protein deposits in human brain tissue: an initial study, *5th International Conference on Advanced Vibrational Spectroscopy/8th Australian Conference on Vibrational Spectroscopy*, July 2009, Melbourne, Australia, pp. 104.

PNG-G, FLOOK-R, NG-B. W.-H AND ABBOTT-D (2009). An initial study of terahertz spectroscopy of human brain tissue, *Alzheimer's Australia National Conference*, June 2009, Adelaide, Australia, pp. 51.

Acknowledgements

In my PhD journey, I have crossed paths with many people—from academics to workshop technicians. Together, these individuals have made my PhD journey memorable, rewarding, and satisfying.

Firstly, I wish to thank my supervisors—Dr Brian W.-H. Ng, Prof. Derek Abbott, and Dr Sam Mickan—at the University of Adelaide for their guidance, enthusiasm, and support of my research. In particular, I wish to thank Prof. Abbott for introducing me to the field of terahertz, and for teaching me to think and write like a researcher.

I had the wonderful privilege to spend five months at Rensselaer Polytechnic Institute (RPI), in Troy, USA. There, I had the honour to meet and work with Prof. Xi-Cheng Zhang, a true pioneer in terahertz technology. I wish to thank him for allowing me to work in his laboratories, and for entrusting me with his priceless THz equipment. At RPI, I had the opportunity to work with Dr Jin-Wook Choi and Dr Ian Guest at the Wadsworth Center (NYS Department of Health, Albany, USA), both of whom provided refreshing advice for my research from medical practitioners' points of view, for which I am grateful. I also thank the staff and students in Prof. Zhang's research teams for their assistance and advice.

A second opportunity to visit an overseas THz group gave me the chance to work for three weeks with Prof. Robert Miles' team at the University of Leeds, UK. I wish to thank Prof. Miles for the unrestricted access to his laboratory, and for making me feel welcomed in his team. My thanks also to Dr Mark Stringer and Dr Mira Naftaly for their technical help with the THz equipment, and their interest in my research.

Back in Australia, I have collaborated with teams both inside and outside my University. I wish to thank Prof. Anton Middelberg and his team at the University of Queensland for introducing me to the world of protein microstructures, and for teaching me how to synthesise proteins. In particular, I am grateful to Dr Robert Falconer for his resourcefulness and enthusiasm. My gratitude extends to Ms Robyn Flook from Flinders University for our collaborative work involving human brain tissue. Her belief in my research has allowed us to make a foray into this uncharted territory.

Within the University of Adelaide, my appreciation extends to Prof. Christophe Fumeaux and Prof. Chris Coleman, both of whom are not involved in my supervision,

Acknowledgements

but have patiently allowed me to bounce ideas off them. I also thank the workshop technicians—the test jigs used to conduct experiments in this Thesis would not exist without them.

I am also grateful to the academics I have had useful discussions with either during their visits to the University of Adelaide, or while at conferences overseas: Prof. Daniel Grischkowsky, Prof. Peter Siegel, Prof. Emma Pickwell-MacPherson, Prof. Milica Popović, Dr Philip Taday, Prof. Vincent Wallace, Dr Andrew Gallant, Dr Peter Swift, and Dr Trevor Bird to name just a few.

Last but not least, I thank my partner, Sheera, whose love, support and belief has sustained me through this PhD journey. I also thank Sheera for proof reading the early versions of this Thesis.

Funding Sources

I wish to extend my heartfelt appreciation to the following funding bodies for giving me the opportunity to (i) conduct my research at the University of Adelaide, (ii) to conduct my research at Rensselaer Polytechnic Institute (RPI), and the University of Leeds; and (iii) to attend various international conferences.

For funding my research: the Australian Postgraduate Award (Australian Research Council); the Cooperative Research Centre for Sensor Signal and Information Processing Scholarship (Australia); the International Society for Optical Engineering (SPIE) Educational Scholarship (USA); the Google Australia and New Zealand Anita Borg Memorial Scholarship (Australia); the Jack Loader Research Scholarship (Australia); the AFUW Fellowship (Australia); the AFUW-SA Daphne Elliott Bursary (Adelaide, Australia); and the AFUW-SA Barbara Crase Bursary (Adelaide, Australia).

For travel funding to RPI, USA: the Mutual Community Postgraduate Travel Grant (University of Adelaide); the Research Abroad Scholarship (University of Adelaide); the AUGU/RC Heddle Award (University of Adelaide); and the International Society for Optical Engineering (SPIE) Educational Scholarship (USA).

For travel funding to the University of Leeds, UK: the Institution of Engineering and Technology (IET) J. R. Beard Travel Award (UK).

For travel funding to various conferences: the Walter and Dorothy Duncan Trust (University of Adelaide); the IEEE South Australia Travel Award (Australia); and the ICAVS/ACOVs Conference student bursary (Monash University, Australia).

Conventions

The following conventions are adopted in this Thesis:

1. **Definitions.** In this Thesis, the terahertz band is defined as being from 0.1–10 THz ($1 \text{ THz} = 10^{12} \text{ Hz}$).
2. **Acronyms and mathematical symbols.** Acronyms and mathematical symbols used in this Thesis are defined on pp. xxxvii–xli, p. 28, and pp. 52–53.
3. **Mathematical units.** The International System of Units (SI) is used throughout this Thesis for units and prefixes.
4. **Spelling.** British English spelling is adopted as default, as defined by the online Oxford English Dictionary (Oxford English Dictionary 2010). American English spelling, where used (e.g. units of length, such as ‘meter’ and ‘submillimeter’; and the technical term ‘program’), is as defined by the online Merriam-Webster Dictionary (Merriam-Webster Dictionary 2010).
5. **Typesetting.** This Thesis is typeset using the $\text{\LaTeX}2\text{e}$ software. Gnu Emacs was used as the word processing interface to $\text{\LaTeX}2\text{e}$.
6. **In-text citation and bibliography referencing.** Harvard style is used for referencing and citation in this Thesis.
7. **Data processing and generation of plots.** Data processing of THz measurements was performed using the MATLAB software, versions 7.5.0 (release R2007b) and 7.6.0 (release R2008a). Manufacturer: the MathWorks Inc. (MathWorks, Inc. 2010). In Chapter 8, the High Frequency Structure Simulator (HFSS, versions 10.1 and 11) software is used in addition to MATLAB. Manufacturer of HFSS: Ansoft (Ansoft 2010).
8. **Colours in schematic diagrams.** In schematic diagrams, THz radiation is depicted in green for convenience, although THz radiation is invisible to the human eye. Laser light is depicted in red.

9. **Generation of schematic diagrams.** Inkscape (version 0.46) and the Gimp (version 2.6.4) were primarily used to create schematics in this Thesis. Adobe Illustrator (version 13.0.0) was used when necessary.
10. **URLs.** The Universal Resource Locators (URLs) of websites used for finding information in this Thesis are provided in the Bibliography Chapter. Access dates are given with each URL to indicate currency.

Nomenclature

Common acronyms used in this Thesis

2D	two dimensional
3D	three dimensional
β -lg	β -lactoglobulin
AC	alternating current
AD	Alzheimer's disease
A β	amyloid- β
CT	computed tomography
CW	continuous wave
DC	direct current
DNA	deoxyribonucleic acid
EO	electro-optic
FDTD	Finite Difference Time Domain
FEL	free electron laser
FEM	Finite Element Method
FFT	fast Fourier transform
FIR	far-infrared
FTIR	Fourier Transform Infrared
FTS	Fourier Transform Spectroscopy
FWHM	full width at half maximum
GaAs	gallium arsenide
GHz	gigahertz
HFSS	High Frequency Structure Simulator
IR	infrared
LIA	lock-in amplifier
MRI	magnetic resonance imaging
NMR	Nuclear Magnetic Resonance
OR	optical rectification
PC	photoconductive
PCA	photoconductive antenna

Common mathematical symbols and constants

QCL	quantum cascade laser
RF	radio frequency
RNA	ribonucleic acid
RPI	Rensselaer Polytechnic Institute
SEM	scanning electron micrograph/microscope
SNR	signal-to-noise ratio
TDS	time domain spectroscopy
TE	transverse electric
TEM	transverse electric and magnetic
TM	transverse magnetic
THz	terahertz (1 THz = 10^{12} Hz)
T-ray, T-rays	terahertz (0.1–10 THz)
ZnTe	zinc telluride

Common mathematical symbols and constants

c	speed of light <i>in vacuo</i>
t	continuous time
ν	frequency
ω	angular frequency = $2\pi\nu$
λ	wavelength
k	wavenumber = $2\pi/\lambda$
\hat{k}	complex wavenumber
i	symbol for complex number
ϵ	electrical permittivity
ϵ_0	electrical permittivity <i>in vacuo</i>
$\hat{\epsilon}$	complex electrical permittivity = $\epsilon' - i\epsilon''$
ϵ'	$\Re\{\text{complex electrical permittivity}\} = \Re\{\hat{\epsilon}\}$
ϵ''	$\Im\{\text{complex electrical permittivity}\} = \Im\{\hat{\epsilon}\}$
μ	magnetic permeability
μ_0	magnetic permeability <i>in vacuo</i>
\hat{n}	complex refractive index = $n - i\kappa$
n	$\Re\{\text{complex refractive index}\} = \Re\{\hat{n}\}$
κ	$\Im\{\text{complex refractive index}\} = \Im\{\hat{n}\}$

σ	conductivity
α	absorption coefficient or extinction coefficient
d	material thickness
ϕ	phase in the frequency domain
T	Fresnel transmission coefficient
R	Fresnel reflection coefficient
e	even
o	odd
W	net rate at which electromagnetic energy crosses a surface
ψ	wave equation symbol
E	scalar electric field
\mathbf{E}	electric field vector
P	scalar polarisation
\mathbf{P}	electric polarisation vector
x	Cartesian or cylindrical x-axis
y	Cartesian or cylindrical y-axis
z	Cartesian or cylindrical z-axis
r	radius of cylinder
ϕ	azimuth
θ	zenith
l	length of cylinder
C	cross section
C_{sca}	scattering cross section
Q	efficiency
Q_{sca}	scattering efficiency
S_{11}	S-parameter (reflection)
S_{21}	S-parameter (transmission)

